Received: 7 January 2018 | Revised: 28 February 2018 | Accepted: 9 April 2018

DOI: 10.4218/etrij.2018-0005

ORIGINAL ARTICLE

WILEY ETRI Journal

Efficient detectors for MIMO-OFDM systems under spatial correlation antenna arrays

David William Marques Guerra | Rafael Masashi Fukuda | Ricardo Tadashi Kobayashi | Taufik Abrão

Electrical Engineering Department, State University of Londrina, Londrina, Paraná, Brazil.

Correspondence
Taufik Abrão, Electrical Engineering Department (DEEL), State University of Londrina, Londrina, Paraná, Brazil.
Email: taufik@uel.br

This work analyzes the performance of implementable detectors for the multiple-input multiple-output (MIMO) orthogonal frequency division multiplexing (OFDM) technique under specific and realistic operation system conditions, including antenna correlation and array configuration. A time-domain channel model was used to evaluate the system performance under realistic communication channel and system scenarios, including different channel correlation, modulation order, and antenna array configurations. Several MIMO-OFDM detectors were analyzed for the purpose of achieving high performance combined with high capacity systems and manageable computational complexity. Numerical Monte Carlo simulations demonstrate the channel selectivity effect, while the impact of the number of antennas, adoption of linear against heuristic-based detection schemes, and the spatial correlation effect under linear and planar antenna arrays are analyzed in the MIMO-OFDM context.

KEYWORDS
BER performance, heuristic detector, linear detector, MIMO-OFDM, multipath channel, spatial correlation

1 | INTRODUCTION

Orthogonal frequency division multiplexing (OFDM) is a modulation scheme widely used in many communication systems, including several commercial applications such as wireless networks (Wi-Fi 802.11) and cellular systems (LTE) [1]. In those systems, it is also common to combine the OFDM with multiple-input multiple-output (MIMO), which can improve the spectral efficiency of the system [2,3]. However, to couple the OFDM to the MIMO system, it is necessary to understand the basics of SISO channel and SISO-OFDM.

Usually, inside an OFDM system, a large number N of subcarriers is deployed in order to achieve a flat fading condition on each subchannel. This is particularly important in realistic scenarios, where the wireless channel introduces dispersion effects on the signal, creating selective channels. In [4], a SISO-OFDM system was simulated to show how the number of subcarriers influences its performance on a multipath fading indoor channel based on the Saleh-Valenzuela model, but not considering the Doppler frequency.

In flat fading channels, the coherence bandwidth of the channel $(\Delta B)_c$ is larger than W, the bandwidth of the signal. Hence, all frequency components of the signal experience the same magnitude of fading. On the other hand, in frequency-selective fading channels, $(\Delta B)_c < W$ occurs. As a consequence, different frequency components of the signal experience correlated fading.

In OFDM systems, to mitigate the intersymbol interference (ISI) caused by multipath fading, it is necessary to use a guard interval. The most used type of guard interval on OFDM systems is the cyclic prefix (CP), as described analytically in [5].

One of the most recent well-established data transmission structures is the multiple-input multiple-output (MIMO) system, which uses multiple antennas at the transmitter and receiver sides to transfer data over a wire or wireless channels. MIMO systems are able to increase data rates by means of multiplexing or to improve performance/reliability through a diversity mode [6]. The data increase can be achieved sending different data via different antennas. By simultaneously sending the same data via multiple antennas, the reliability is increased by exploiting diversities such as time and space diversity. In spatial multiplexing, the signal that reaches at each receive antenna suffers interference from the other $N_t - 1$ antennas, where N_t represents the number of transmitting antennas. Hence, the purpose of demultiplexing-detection schemes is to mitigate the effects of the interference [7]. Hence, on the receiver side, there are a large number of MIMO detection techniques available. In this work, several MIMO-OFDM detectors are characterized and numerically evaluated under specific but realistic channel and system scenarios, including the maximum likelihood (ML), linear zero-forcing (ZF), and linear minimum mean-square error (MMSE) detectors. Moreover, two MIMO-OFDM detectors based on evolutionary heuristic approaches also have been analyzed, namely, the *particle swarm optimization* (PSO) detector and *differential evolution* (DE) detector.

Indeed, because the ML detector solution requires an exhaustive search through all possible symbol combinations [8], while linear closed solutions such as ZF and MMSE result in a poor performance for highly correlated channels [9], evolutionary heuristic algorithms are strong candidates for producing better solutions than linear detectors, and they result in reduced computational complexity compared to ML because heuristic approaches do not evaluate all possibilities.

The PSO algorithm has already been applied to solve the detection problem in MIMO-OFDM systems in [8,10]. In [8], the PSO, and in [11], the binary PSO, were evaluated and the numerical results of bit error rate (BER) and computational complexity were analyzed. In [10], the performances of DE, PSO, and the genetic algorithm were compared. On the other hand, in our work, the performance-complexity tradeoff of the evolutionary heuristic PSO and DE MIMO-OFDM detectors are analyzed under practical and useful scenarios, that is, considering spatial correlated channels and other linear conventional MIMO-OFDM detectors. The system model in a real-valued representation is considered while the selection procedure for the heuristic input parameters of the PSO and DE algorithms are addressed accordingly. Besides, to the best of our knowledge, there are no studies considering a comparative analysis of evolutionary heuristics and classical MIMO-OFDM detectors operating under spatial correlation antenna arrays.

The contribution of this work is threefold. First, we analyze and compare the performance and implementability of several MIMO-OFDM detectors, including linear and evolutionary heuristic approaches, operating under realistic system configurations. Second, the influence of parameters related to the distance between the antennas, which determine the spatial antenna correlation, is discussed; two antenna array configurations are considered, the *uniform linear array* (ULA) [12] and *uniform rectangular array* (URA) [13]. Last, a systematic procedure is developed and used to calibrate the input parameters of both evolutionary heuristic PSO and DE detectors with the aim of establishing a fair performance comparison between the linear and heuristic MIMO-OFDM detectors.

The rest of this work is organized as follows. In Section 2, the OFDM system is revised and the TD channel emulator is explored. The spatial channel correlation, ML, ZF, MMSE, as well as the evolutionary heuristic PSO and DE detectors are described in Section 3. Extensive numerical simulation results are analyzed in Section 5, including reliability evaluation, the channel selectivity effect, BER performance comparison regarding spatial correlation, modulation order, and sensibility analysis. Conclusions and final remarks are offered in Section 6.

2 | OFDM TRANSMISSION AND MIMO CHANNEL

OFDM is one type of multicarrier modulation that can be easily implemented using discrete Fourier transform (DFT) and its inverse (IDFT), or their equivalents, the fast Fourier transform (FFT) and inverse FFT (IFFT). OFDM modulation consists of parallel data transmission with some modulation such as M-QAM or M-PSK applying an IFFT to transform a signal in the FD into one in the TD. Thereafter, the CP is added. Data are converted into an analog signal. Finally, the signal is multiplied to a carrier by frequency f_c for transmission.

On the receiver side, signal $r(t)$ represents the transmitted signal $s(t)$ corrupted by noise. Signal $r(t)$ is multiplied by $\cos(2\pi f_c t)$, passes through a low-pass filter, is converted to digital information, the CP is removed, and the serial data is converted into parallel data. A DFT is performed, the symbols are converted to serial symbols and demodulated according to their respective scheme of modulation, and the information bits can then be estimated.

In order to mitigate ISI, some strategies such as cyclic suffix, silence, or the most common CP can be adopted.

CP consists of copying the last μ elements of the input sequence $s[n]$ and adding them to the start of $s[n]$, where $h[n] = h[0], h[1], \ldots, h[\mu]$ represents a channel impulse response of length $\mu + 1$. After the CP addition, the OFDM symbol becomes $\tilde{s}[n]$, with length $[N + \mu]$. Observe

that the CP is an overhead and does not carry any information, which reduces the spectral efficiency.

The choice of the number of subcarriers N depends on the channel characteristics. For the design of an OFDM system, two properties of the channel are considered, which are the maximum delay spread (τ_{max}) and the maximum Doppler frequency (f_d). OFDM systems require that N must be large enough so each subcarrier experiences a flat fading condition. Each subcarrier has a bandwidth B that is smaller than the system total bandwidth, centered at a frequency $\omega_1, \omega_2, \ldots, \omega_n$. Subcarriers with a bandwidth of B can be overlapped at a maximum rate of 50%.

2.1 | MIMO-OFDM system

The combination of an OFDM system with the use of multiple antennas at the transmitter and receiver results in a MIMO-OFDM system (Figure 1) with N_t transmit and N_r receive antennas. A QAM modulator and multiplexing configuration, where different data are sent through different antennas resulting in higher data rates than single-input single-output (SISO) channel configuration, have been considered.

On the transmitter side, the data feeds a serial-to-parallel converter, resulting in N_t data streams that are modulated in a similar way as OFDM SISO: the bit stream is modulated, symbols are converted to parallel, IDFT is performed, the CP is added, and the signal is multiplied by the carrier with frequency f_c and finally transmitted. On the receiver side, the signal is converted to baseband, transformed into digital, the CP is removed, the signals serve as a MIMO detector, and finally, the symbols are demodulated deploying QAM demodulator.

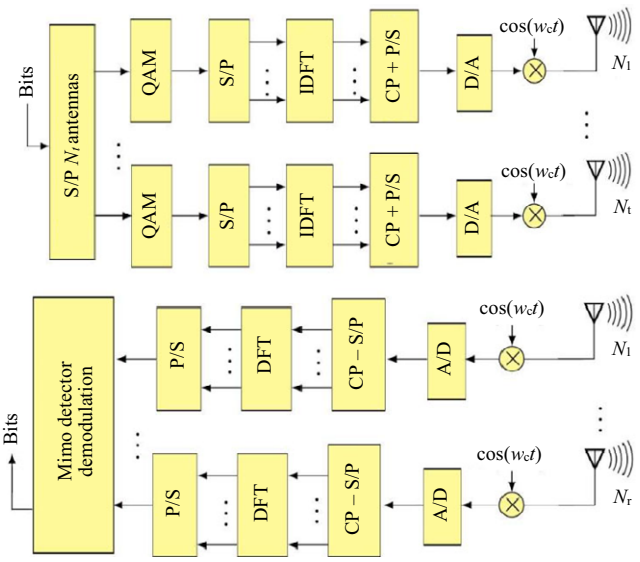

FIGURE 1 Block diagram of a MIMO-OFDM system

Because the OFDM technique allows parallel transmission over several subchannels, we can model a MIMO-OFDM system with N subcarriers in the TD as [14,15]:

$$\mathbf{y}[n] = \mathbf{H}[n]\mathbf{x}[n] + \mathbf{z}[n], \quad n = 0, 1, \ldots, N-1, \tag{1}$$

where n is the subcarrier index, $\mathbf{y}[n] \in \mathbb{C}^{N_r \times 1}$ denotes the received signals, $\mathbf{H}[n] \in \mathbb{C}^{N_r \times N_t}$ denotes the channel matrix gains, $\mathbf{x}[n] \in \mathbb{C}^{N_t \times 1}$ denotes the transmit symbols, and $\mathbf{z}[n] \in \mathbb{C}^{N_r \times 1}$ is Gaussian noise with zero mean and variance σ_z^2.

Therefore, we can interpret a MIMO system for each subcarrier, as illustrated in Figure 2. Thus, a MIMO-OFDM symbol block is composed of $N_r \times N_t$ OFDM symbols. Finally, it is important to note that if the number of subcarriers is insufficient to make the channel of each subcarrier flat, channel equalization cannot be implemented correctly.

Implementable MIMO-OFDM detectors operating in realistic fading channels and practical system configuration are discussed in Section 3.

3 | MIMO SPATIAL CORRELATION AND LINEAR DETECTORS

3.1 | MIMO-OFDM spatial correlation model

In channel modeling, the correlation among transmit and/or receive antennas is an important aspect to be considered in realistic MIMO channels and systems [16]. To model and evaluate the spatial antenna correlation, the Kronecker operator is deployed as:

$$\mathbf{H}_{corr}[n] = \sqrt{\mathbf{R}_r}\mathbf{G}[n]\sqrt{\mathbf{R}_t^H}, \tag{2}$$

where $\mathbf{H}_{corr}[n]$ is the correlated channel of the nth subcarrier, uncorrelated channel matrix $\mathbf{G}$ is composed of independent and identically distributed entries, $\sqrt{\mathbf{R}_r}$ and $\sqrt{\mathbf{R}_t}$ are the square root of the spatial correlation matrices at the transmitter and receiver antennas, respectively.

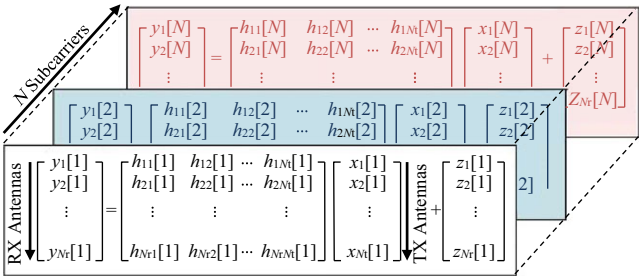

FIGURE 2 MIMO-OFDM problem

3.2 | Uniform linear antenna array (ULA)

A spatial correlation model for ULA was proposed in [12]. This model considers that the antennas are arranged equidistantly, where d_t and d_r represent the spacing between the transmitting and receiving antennas, respectively. For simplicity of analysis, assuming the same number of antennas at the transmitter and receiver ($N_t = N_r$) side, while the spatial correlation matrix of the transmitter and receiver antennas are assumed to be equal $\sqrt{\mathbf{R}_r} = \sqrt{\mathbf{R}_t}$. The spatial correlation matrix results Toeplitz, being expressed by:

$$\mathbf{R}_t = \mathbf{R}_r = \begin{bmatrix} 1 & \rho & \rho^4 & \cdots & \rho^{(N_t-1)^2} \\ \rho & 1 & \rho & \ddots & \vdots \\ \rho^4 & \rho & 1 & \cdots & \rho^4 \\ \vdots & \vdots & \vdots & \cdots & \rho \\ \rho^{(N_t-1)^2} & \cdots & \rho^4 & \rho & 1 \end{bmatrix} \quad (3)$$

where $\rho \in [0, 1]$ represents the normalized correlation index between antennas.

3.3 | Uniform rectangular antenna array (URA)

An approximation for the URA correlation model was proposed in [13]. This model assumes that the URA matrix correlation between the antennas is obtained from the Kronecker product of 2 ULA correlation matrices. Considering an URA configuration on the XY plane with n_x and n_y antenna elements along X and Y coordinates, respectively, we have an array with $n = n_x \times n_x$ antennas. Further, the correlation between the elements along the X coordinate does not depend on Y and is given by matrix $\mathbf{R}_x$, and the correlation along Y coordinate does not depend on X and is given by matrix $\mathbf{R}_y$. As a result, the Kronecker model approximation for the URA correlation matrix is as follows:

$$\mathbf{R}_r = \mathbf{R}_x \otimes \mathbf{R}_y, \quad (4)$$

where $\otimes$ is the Kronecker product.

3.4 | Maximum likelihood (ML) MIMO detector

The ML detector provides the best performance, but its complexity makes it impractical for real applications. This detector calculates all the possible symbols combinations and chooses the one symbol vector $\mathbf{x}$ that provides the minimum Euclidian distance between the received data $\mathbf{y}$ and the reconstructed data defined by the channel matrix $\mathbf{H}$ and symbol-vector candidate $\mathbf{x}$. Hence, the estimated symbol $\tilde{\mathbf{x}}$ can be mathematically expressed by

$$\tilde{\mathbf{x}} = \min_{\mathbf{x}} \|\mathbf{y} - \mathbf{H}\mathbf{x}\|^2. \quad (5)$$

3.5. | Zero-forcing (ZF) MIMO detector

Considering a MIMO system operating under multiplexing mode, the data that reach the receptor are the linear superposition of the signals of all the N_t antennas [7]. The ZF detector ignores the additive noise $\mathbf{z}$ in (1) and solves the linear system by multiplying the received signal by the inverse matrix, which is defined, according to the Moore–Penrose inverse, as:

$$\mathbf{H}_{zf}^{\dagger} = (\mathbf{H}^H\mathbf{H})^{-1}\mathbf{H}^H. \quad (6)$$

The estimated symbol is given by

$$\tilde{\mathbf{x}} = \mathbf{H}_{zf}^{\dagger}\mathbf{y}. \quad (7)$$

3.6 | Minimum mean-square error (MMSE) MIMO detector

The MMSE detector considers the thermal noise channel statistics. This method tries to minimize the squared error between the true and estimated values of the transmitted symbols, $\mathbf{x}$ and $\tilde{\mathbf{x}}$, respectively [7] via optimization

$$\mathbf{H}_{mmse}^{\dagger} = \min_{\mathbf{W}} \mathbb{E}\|\mathbf{x} - \mathbf{W}\mathbf{y}\|. \quad (8)$$

Hence, solving this MMSE optimization problem, the MIMO channel matrix results in the MMSE pseudoinverse matrix described by

$$\mathbf{H}_{mmse}^{\dagger} = \left(\mathbf{H}^H\mathbf{H} + \frac{N_0}{E_s}\mathbf{I}\right)^{-1}\mathbf{H}^H, \quad (9)$$

where $\frac{N_0}{E_s}$ is the inverse of the signal-to-noise ratio (SNR). Finally, the estimated symbol under linear MMSE MIMO detection is obtained in the same way as in (7) and is give by:

$$\tilde{\mathbf{x}} = \mathbf{H}_{mmse}^{\dagger}\mathbf{y}. \quad (10)$$

4 | HEURISTIC-BASED MIMO-OFDM DETECTORS

In this section, the heuristic PSO and DE algorithms are described in the context of the MIMO-OFDM detection problem. The complex system model is described in a well-known equivalent real-valued representation, for example, in [17]. The deployment of the fitness function to evaluate the candidate solution provided by heuristic

algorithms is illustrated. PSO and DE algorithms are presented afterwards, while the input parameter tuning problem for the evolutionary heuristic algorithms is addressed.

4.1 | Real value representation

The MIMO-OFDM system presented in (1) can be represented using a real-valued matrix and vectors in the form

$$\boldsymbol{\upsilon}[n] = \mathcal{H}[n]\boldsymbol{\gamma}[n] + \boldsymbol{\xi}[n], \tag{11}$$

with

$$\mathcal{H}[n] = \begin{bmatrix} \Re\{\mathbf{H}[n]\} & -\Im\{\mathbf{H}[n]\} \\ \Im\{\mathbf{H}[n]\} & \Re\{\mathbf{H}[n]\} \end{bmatrix}, \boldsymbol{\upsilon}[n] = \begin{bmatrix} \Re\{\mathbf{y}[n]\} \\ \Im\{\mathbf{y}[n]\} \end{bmatrix},$$
$$\boldsymbol{\gamma}[n] = \begin{bmatrix} \Re\{\mathbf{x}[n]\} \\ \Im\{\mathbf{x}[n]\} \end{bmatrix}, \boldsymbol{\xi}[n] = \begin{bmatrix} \Re\{\mathbf{z}[n]\} \\ \Im\{\mathbf{z}[n]\} \end{bmatrix},$$

where $\mathcal{H}[n] \in \mathbb{R}^{2N_r \times 1}$ is the real-valued representation of the channel matrix, vectors $\boldsymbol{\gamma}[n]$, $\boldsymbol{\xi}[n] \in \mathbb{R}^{2N_r \times 1}$ are the real-valued representations of the received signal and additive noise, respectively, and $\boldsymbol{\upsilon}[n] \in \mathbb{R}^{2N_r \times 1}$ is the real-valued original information.

4.2 | Fitness function

The fitness function evaluates the quality of the estimated symbol and guides the evolutionary heuristic search on the candidate-solution feasible subspace. For the detection problem, the fitness function is based on the Euclidean distance between the received signal and the reconstructed one [8,10,11]. Considering $\boldsymbol{\zeta}_k$, the kth candidate solution of an evolutionary heuristic, namely a particle in PSO or individual in DE, the fitness function is calculated as follows:

$$f(\boldsymbol{\zeta}_k) = \|\boldsymbol{\upsilon}[n] - \mathcal{H}[n]\boldsymbol{\zeta}_k\|^2. \tag{12}$$

For the detection problem, a minimization problem is considered, and lower values of the fitness function are desired.

4.3 | PSO-based detection algorithm

PSO was proposed by [18] considering a population-based approach, emulating bird flocking and fish schooling behavior. The PSO algorithm calculates the velocity and position of each particle inside the swarm; using a matrix representation [19], they are given, respectively, by

$$\mathbf{V} = w\mathbf{V} + c_1\mathbf{U}_1 \odot (\mathbf{M}_{\text{pb}} - \mathbf{P}) + c_2\mathbf{U}_2 \odot (\mathbf{M}_{\text{gb}} - \mathbf{P}), \tag{13}$$

and

$$\mathbf{P} = \mathbf{P} + \mathbf{V}, \tag{14}$$

where $\odot$ denotes the Hadamard product, w, c_1, and c_2 represent inertia, cognitive, and social factors, respectively; $\mathbf{U}_1$ and $\mathbf{U}_2$ are random matrices with elements following uniform distributions $\mathbf{U}_i \sim \mathcal{U}[0;1]$; $\mathbf{M}_{\text{pb}}$ is a matrix that stores the values of the personal best of each particle and $\mathbf{M}_{\text{gb}}$ is a matrix constructed of the positions of the global best particle $\mathbf{p}_{\text{gb}}$, given in the form $\mathbf{M}_{gb} = [\mathbf{p}_{\text{gb}} \cdots \mathbf{p}_{\text{gb}}] \in \mathbb{R}^{N_{\text{dim}} \times N_{\text{pop}}}$. Matrix $\mathbf{P}$ is a real-valued matrix representing positions, while $\mathbf{V}$ represents the particle velocity matrix; explicitly,

$$\mathbf{P} = [\mathbf{p}_1 \ldots \mathbf{p}_{N_{\text{pop}}}], \mathbf{V} = [\mathbf{v}_1 \ldots \mathbf{v}_{N_{\text{pop}}}] \in \mathbb{R}^{N_{\text{dim}} \times N_{\text{pop}}},$$

where vectors $\mathbf{p}_k, \mathbf{v}_k \in \mathbb{R}^{N_{\text{dim}} \times 1}$ with $k = 1, \ldots, N_{\text{pop}}$ represent the position and velocity of the kth particle, with N_{pop} representing the population size and N_{dim} denoting the dimensionality of the problem.

In order to avoid the possibly that the velocity vector grows to infinity [20], a limitation of the velocity [$-V_{\max}$, $V_{\max}$] [21] was considered, where $V_{\max}$ represents the maximum achievable velocity of the N_{pop} particles. Regarding the inertia parameter, it can be a constant or a linear or nonlinear function [22]. In this work, to give to the algorithm exploitation ability at the beginning and exploration for fine search near the solution [21], a strategy of decreasing the inertia factor at each iteration by $0.99w$ is considered.

The initialization of both implemented PSO and DE heuristic algorithms was the same; the position of the particles $\mathbf{P}$ and initial population in DE are generated randomly following a uniform distribution inside the search space of the problem [23]. These positions are set as the personal best position of the particle in matrix $\mathbf{M}_{\text{pb}}$. The fitness function in (12) is evaluated ($\boldsymbol{\zeta}_k = \mathbf{p}_k$, $k = 1, \ldots, N_{\text{iter}}$), the position of the particle that produces the lowest value (since we are dealing with a minimization problem) is set as the global best position $\mathbf{p}_{\text{gb}}$, and the matrix $\mathbf{M}_{\text{gb}}$ is formed.

After evaluation of (13) and (14), matrices $\mathbf{M}_{\text{pb}}$ and $\mathbf{M}_{\text{gb}}$ are updated (if needed) and the process is repeated until the stop criteria is met. In our implementation, a stop criterion based on a predefined maximum number of evaluations N_{iter} is used. Hence, after N_{iter} iterations, the output of the evolutionary heuristic algorithm is the vector of best position $\mathbf{p}_{\text{gb}}$, which is the estimated symbol $\tilde{\mathbf{x}}$ in the MIMO-OFDM detection problem.

Pseudocode summarizing the procedure for the evolutionary heuristic PSO algorithm is presented in Algorithm 1.

Algorithm 1. PSO

1: Input parameters: c_1, c_2, w, N_{pop}, N_{iter}
2: Generate initial positions $\mathbf{P}$
3: Fitness function evaluation and initialization of $\mathbf{M}_{\text{pb}}$ and $\mathbf{M}_{\text{gb}}$
4: for 1 to N_{iter} do
5: Calculate velocity using (13)
6: Calculate position using (14)
7: Evaluate fitness function (12) for all particles p_k
8: Update personal best matrix $\mathbf{M}_{\text{pb}}$
9: Update global best matrix $\mathbf{M}_{\text{gb}}$
10: Velocity limitation
11: Inertia factor reduction
12: end for
13: Output: $\mathbf{p}_{\text{gp}}$

4.4 | DE-based detection algorithm

DE is an evolutionary population-based heuristic that relies on a population of individuals to find a global optimum. The algorithm relies on the operations of mutation, crossover, and selection to produce more suitable individuals through N_{gen} generations.

The DE algorithm was presented in [23] and operates as follows. There are $N_{\text{ind}} \geq 4$ vectors of individuals that are represented as $\boldsymbol{\iota}_k \in \mathbb{R}^{N_{\text{dim}} \times 1}, k = 1, \ldots, N_{\text{ind}}$, where N_{dim} represents the dimensionality of the problem. Here, following the procedure defined in [23], the `rand/1/bin` strategy is employed. Strategies to escape local optima that are adopted in the DE-based detector are described in the following.

4.4.1 | Mutation

The kth mutation vector $\boldsymbol{\upsilon}$ is constructed as:

$$\boldsymbol{\upsilon}_k = \boldsymbol{\iota}_{r_1} + F_{\text{mut}}(\boldsymbol{\iota}_{r_2} - \boldsymbol{\iota}_{r_3}), \tag{15}$$

where $k \neq r_1 \neq r_2 \neq r_3$ and $k = 1, \ldots, N_{\text{ind}}$. Variables r_1, r_2, and r_3 are integer random indexes uniformly distributed inside the interval $[1, 2, \ldots, N_{\text{ind}}]$ and $F_{\text{mut}} \in [0, 2]$ represents the mutation scale factor.

4.4.2 | Crossover

The kth crossover vector $\boldsymbol{\psi}_k (k = 1, \ldots, N_{\text{ind}})$ is constructed as follows. The ith element, $i = 1, \ldots, N_{\text{dim}}$ of the kth crossover vector $\boldsymbol{\psi}_k$ is selected given the following rule:

$$\psi_{ik} = \begin{cases} \nu_{ik} & \text{if } rand \in [0,1] \leq F_{\text{cr}} \text{ or } i = r_4 \\ \iota_{ik} & \text{if } rand \in [0,1] > F_{\text{cr}} \text{ and } i \neq r_4 \end{cases} \tag{16}$$

where $rand \sim \mathcal{U}[0,1]$, r_4 is uniformly distributed in the interval [0;1], r_4 is an integer randomly generated in the interval $[1, \ldots, N_{\text{dim}}]$, and the crossover factor is defined by $F_{\text{cr}} \in [0, 1]$. As pointed out in [23], the crossover vector has at least one element from the mutation vector, that is, $i = r_4$.

4.4.3 | Selection

The next generation of individuals $\boldsymbol{\iota}_k^g$ is constructed as follows:

$$\boldsymbol{\iota}_k^g = \begin{cases} \boldsymbol{\psi}_k & \text{if } f(\boldsymbol{\psi}_k) < f(\boldsymbol{\iota}_k) \\ \boldsymbol{\iota}_k & \text{otherwise} \end{cases}. \tag{17}$$

The fitness function in (12) evaluates $\boldsymbol{\iota}_k$ and $\boldsymbol{\psi}_k$. Vectors that produce more suitable values (smaller values) are selected and a new generation of individuals is produced.

After the execution of N_{gen} iterations, the best individual, in other words, the individual corresponding to the lowest value of the fitness function in (12) is the output of the algorithm and the estimated symbol $\tilde{\mathbf{x}}$ of the MIMO-OFDM detection problem. Pseudocode synthesizing the DE steps is presented in Algorithm 2.

Algorithm 2 DE

1: Input parameters: F_{cr}, F_{mut}, N_{ind}, N_{gen}
2: Generate initial individuals
3: for 1 to N_{gen} do
4: Mutation using (15), $k = 1, \ldots, N_{\text{ind}}$
5: Crossover using (16), $i = 1, \ldots, N_{\text{ind}}$; $k = 1, \ldots, N_{\text{ind}}$
6: Select new individuals using (17), $k = 1, \ldots, N_{\text{ind}}$
7: end for
8: Output: best individual $\boldsymbol{\iota}$

4.5 | Input parameters

The choice of nonoptimal input parameter values could substantially degrade the performance results provided by the heuristic algorithm in a given application, as studied in [24] for the ant colony optimization algorithm. Besides, the PSO algorithm also suffers from alteration of its convergence properties when the input parameters are chosen incorrectly [20,25,26]. In the same way, the DE-based algorithm has recommended intervals of values to achieve fast convergence [23]. For instance, the number of individuals must be $N_{\text{ind}} \in \{5;10\}N_{\text{ind}}$, where N_{dim} is the problem dimension, as suggested in [23].

To fairly compare the selected evolutionary heuristic algorithms, and since such an approach is sensible with respect to the choice of the input parameter values, which can differ substantially considering the nature of different optimization problems, the input parameter tuning

procedure here is obtained numerically and discussed in Sections 5.1.1 and 5.1.2.

5 | NUMERICAL RESULTS

In this section, numerical simulation results of MIMO-OFDM system are discussed. Linear and evolutionary heuristic detector performance subject to spatial antenna correlation effect is compared.

5.1 | MIMO-OFDM reliability evaluation

The parameters adopted in the Monte Carlo simulations are shown in Table 1. Additionally, the system operates with perfect channel state information (CSI). Performance of such detectors is compared with the optimum maximum-likelihood (ML) MIMO-OFDM detector. The total power allocated was equally distributed (EPA) among the N_t antennas in order to promote a fair comparison.

TABLE 1 MIMO-OFDM simulation parameters

Parameter	Value
OFDM	
System bandwidth BW	20 MHz
Modulation order M	4-QAM
Delay spread τ_{rms}	5 1ns
# subcarriers N	64
$(\Delta B)_c$	3.125 MHz
Subcarrier flatness $\frac{(\Delta B)_c}{W/N}$	10
MIMO	
# antennas $N_t \times N_r$	2×2; 4×4; 8×8
Antenna array type	Linear (ULA); rectangular (URA)
Spatial correlation index	$\rho \in [0; 0.5; 0.9]$
Linear detectors	ZF & MMSE
Heuristic detectors	PSO & DE
Power allocation strategy	EPA
Channel	
Type	NLOS rayleigh channel
CSI knowledge	Perfect
Mobility (freq. Doppler)	$f_d = 0$ Hz
PSO detector	
Population size N_{pop}	40
Iterations N_{max}	100
Search space	$[-1; 1]$
Cognitive factor c_1	4
Social factor $c_2(\rho)$	1(0); 0.5(0.5); 1(0.9)
Inertia $w(\rho)$	1.5(0); 1.5(0.5); 3.5(0.9)
DE detector	
# generation N_{gen}	100
Crossover factor $F_{cr}(\rho)$	0.6(0); 0.6(0.5); 0.8(0.9)
Mutation factor $F_{mul}(\rho)$	0.6(0); 0.8(0.5); 1.8(0.9)
# individuals N_{ind}	40

Specifically, in the MIMO-OFDM detection problem with heuristics, a 4-QAM modulation format was considered, with valid symbols defined by $\{-1+1j, -1-1j, 1+1j, 1-1j\}$, while the search space was limited to the interval of integer values $[\pm 1]$. The heuristic algorithm was applied to each subcarrier as presented in the model description in (11), resulting in $N_{dim} = 2N_t$ symbols to be estimated per subcarrier. For the PSO detection algorithm, parameter $V_{max} = 1$ was used in the simulations, reflecting the dynamic range of each particle inside the search space [21].

5.1.1 | Input parameter calibration for PSO-aided MIMO-OFDM detector

First, a round of simulations was executed to tune the PSO input parameters. Here, these parameters were obtained numerically over 100 simulation runs and averaged to obtain the values in Figure 3. The start parameters were $N_{pop} = 40$, $c_1 = c_2$, $w = 1$, and $N_{iter} = 50$. In Figure 3, the PSO input parameters were altered considering a wide range of input parameter values. The scenario assumed was 4×4, 4-QAM modulation MIMO-OFDM, considering a system operating in a medium-high SNR, that is, $E_b/N_0 = 24$ dB, and different values of spatial correlation. Choosing PSO parameters that provide small values of BER yielded the input parameters shown in Table 1 and deployed in the numerical simulation setup discussed in this section. Related to the population size, even with a marginal decrease in BER, low values of N_{pop} are desirable because this parameter has a direct impact in the computational complexity of the algorithm, as detailed in Section 5.2.

In Figure 4, the convergence behavior for the PSO-based detector is analyzed. It can be observed that convergence depends on the level of E_b/N_0; the number of iterations for convergence increases with SNR, from $\approx$ 25 to 50 iterations when E_b/N_0 increases from 5 dB to 10 dB and 15 dB. Moreover, high values of spatial correlation ($\rho = 0.9$) seem to interfere substantially in the convergence speed of the PSO algorithm applied in the MIMO-OFDM detection problem. After around 40 iterations, there are small improvements in the solution (symbol detection) provided by PSO algorithm for any spatial correlation level.

5.1.2 | Input parameter calibration DE-aided MIMO-OFDM detector

A similar procedure was carried out to find the best input parameter values of the DE-based detector in the context of

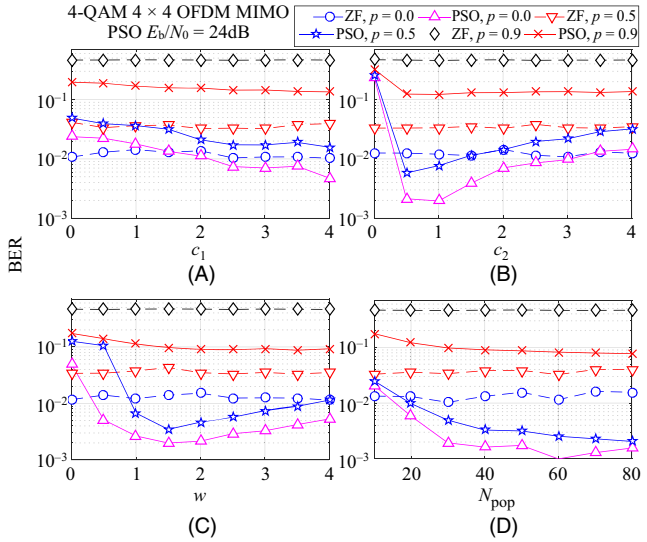

FIGURE 3 Calibration of PSO input parameter values for 4-QAM 4 × 4 MIMO-OFDM detection problem operating under medium-high SNR and different spatial correlation indexes

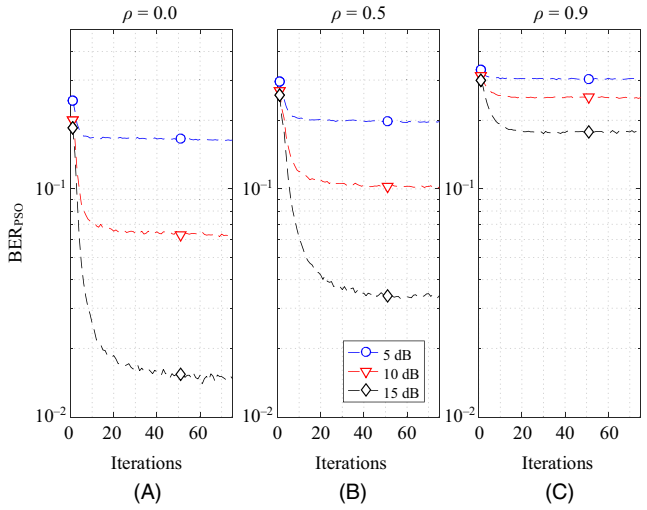

FIGURE 4 Convergence analysis for a 4-QAM, 4 × 4 MIMO-OFDM with PSO detector considering different values of E_b/N_0

MIMO-OFDM detection. This algorithm requires the parameters to be inside the intervals $F_{cr} \in [0, 1]$ and $F_{mul} \in [0, 2]$. Moreover, $N_{ind} \geq 4$ and it is recommended [23] that N_{ind} be between $5N_{dim}$ and $10N_{dim}$. The selected input parameters values were chosen to be those that minimize the BER and are presented in Table 1. Note that the optimum mutation factor value increases with antenna correlation index ρ. Figure 5 depicts the simulated BER curves for a wide range of input parameter values, showing the best values of such input parameters, that is, those values that minimize the BER. The calibration procedure is finished when the range of those input parameters is narrowed.

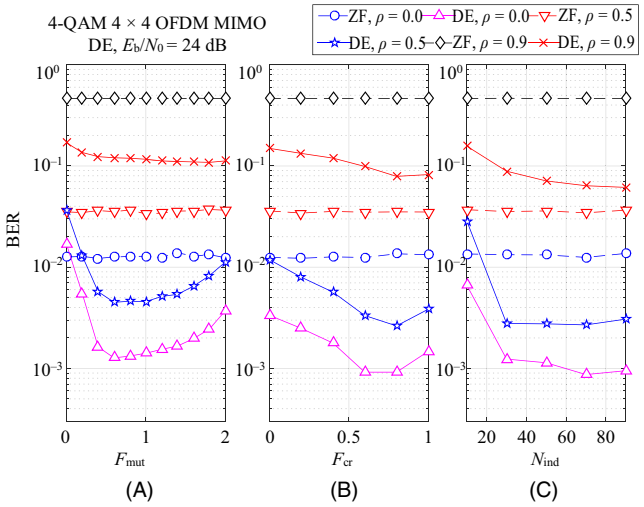

FIGURE 5 Calibration of the input parameters for the DE-aided MIMO-OFDM detector algorithm considering different values of spatial correlation

After the input parameter tuning procedure, the convergence of the DE-aided OFDM-MIMO detector algorithm is obtained, as depicted in Figure 6. Similar to the PSO convergence behavior, the convergence of the DE detector seems to be attained at around 40 iterations, being influenced mainly by the E_b/E_0 levels.

5.1.3 | Effect of spatial correlation on performance

In this section, the numerical simulation results for the BER performance were obtained under different correlation index ρ values, which represents the antenna separation on the transmitter and receiver sides, as depicted in Figure 7. As inferred previously from Figures 4 and 3, the spatial correlation deteriorates the BER performance; as ρ

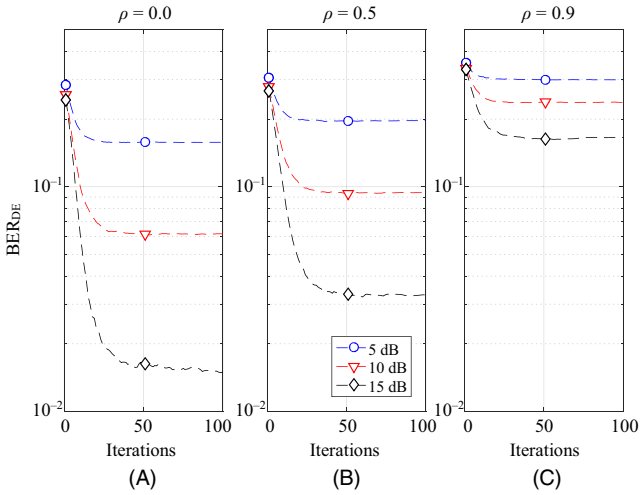

FIGURE 6 Convergence of the DE-aided detector for MIMO-OFDM systems for different spatial correlation values

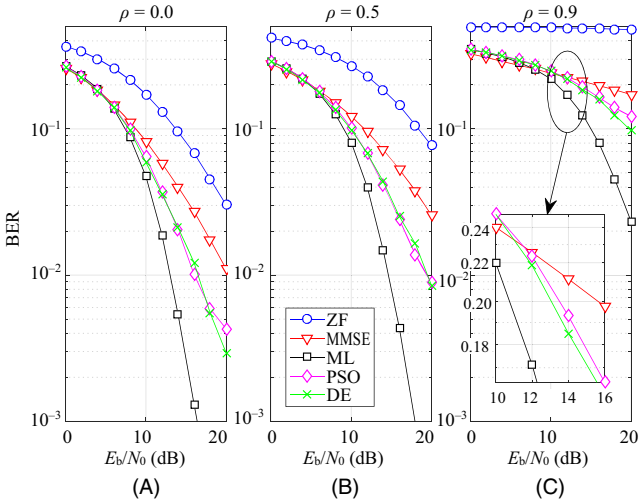

FIGURE 7 BER performance for 4-QAM, 4 × 4 ULA antenna MIMO-OFDM detectors under different values of spatial correlation and SNR

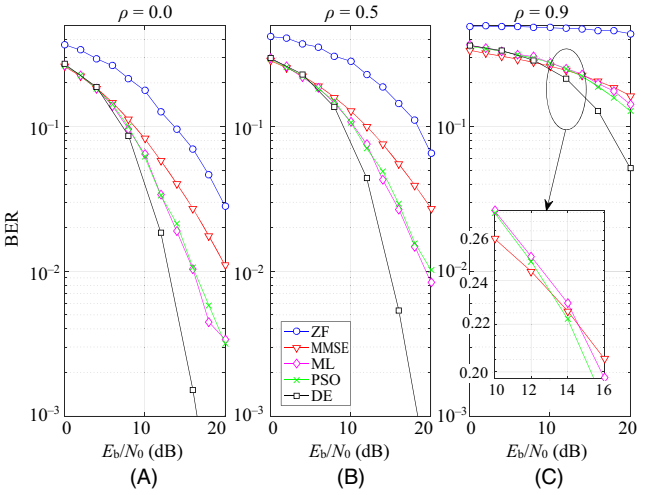

FIGURE 8 BER performance for 4-QAM 4 × 4 OFDM MIMO with linear and heuristic detectors for a URA configuration and different values of correlation and SNR

increases, the probability of error also increases. Under the most highly correlated channels $\rho = 0.9$, the ZF detector provides an unacceptable performance, even operating within the high E_b/E_0 region. The effect of degradation of spatial correlation on the performance also influences the ML detector's performance; however, the ML detector still attains a suitable performance considering uncoded system, at the cost of an enormous computational complexity. Alternatively, considering low-complexity evolutionary DE-based and PSO-aided detectors under the $\rho = 0$ scenario, PSO can outperform MMSE; however, in a highly correlated situation, this performance advantage becomes marginal, while the DE-based MIMO-OFDM detector performs marginally worse than MMSE for all SNR regions. Hence, under medium or even highly correlated MIMO channels, the linear MMSE and the PSO-based detectors represent good options regarding the performance-complexity tradeoff in MIMO-OFDM systems.

Figure 8 explores the BER performance considering planar arrays (URA) instead of a ULA. For high E_b/E_0, medium ρ, and a low number of antennas (4 × 4), the planar array configuration slightly outperforms the linear array design for ZF, MMSE, and PSO detectors (compare the BER performance of Figures 7 and 8). Note that the use of a URA system implies a slightly higher correlation among antennas compared to the ULA. Despite this, the URA performance remains very similar to that of the ULA and is even slightly better at high SNR.

5.1.4 | Sensitivity analysis

To compare the BER degradation with respect to array antenna correlation, the sensitivity of the detectors' performance regarding the level of correlation can be defined as:

$$\kappa_{\text{scn}} = \log_{10} \text{BER}_{\text{scn}} - \log_{10} \text{BER}_{\text{ref}}, \tag{18}$$

where BER_{ref} represents the reference BER value, and BER_{scn} is the BER in a specific scenario, including spatial correlation conditions or detector type.

For illustration purposes, two cases are studied: the degradation in performance when comparing the BER of each detector with respect to uncorrelated antennas ($\rho = 0$); and the degradation using the ML detector as a reference, since its performance is superior to that of the others. Figure 9 depicts both sensitivity scenarios.

κ_ρ: In Figure 9A, the sensitivity considering the performance of each detector at $\rho = 0$ as the correlation increases

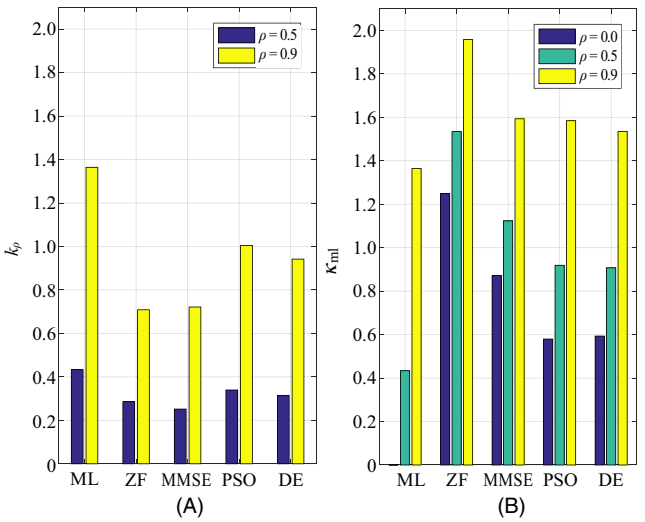

FIGURE 9 Sensitivity of detectors for two correlation scenarios: (A) κ_ρ, comparing each detector with its BER under $\rho = 0$ and (B) κ_{ml}, comparing detector performance with ML detector performance under $\rho = 0$

was numerically obtained. Hence, comparing the performance degradation sensitivity for each detector at $\rho = 0.5$ and $\rho = 0.9$, one can conclude that ML's sensitivity to increasing channel correlation is severely degraded compared with that of the linear and heuristic detectors because of its excellent performance under the $\rho = 0$ condition; while for the ZF detector, the degradation is small, since it already has poor performance compared to the other detectors. In short, the four MIMO-OFDM detectors are not robust to the spatial correlation channel effect.

κ_{ml}: In Figure 9B, sensitivity is shown, taking the ML detector BER performance with $\rho = 0$ as reference BER_{ref}. For medium correlation values ($\rho = 0.5$), the PSO is most near to ML's sensitivity performance degradation, and so κ_{ml} has relatively low results. For $\rho = 0.9$, the ZF detector performs poorly in terms of BER, resulting in a high sensitivity index κ_{ml}. The PSO-aided detector is more sensitive in terms of κ_ρ because its BER varies more as correlation increases, but less sensitive in terms of κ_{ml}, mainly for low and medium spatial correlation channel indexes ($\rho \leq 0.5$).

5.2 | Complexity analysis

To evaluate the complexity of the algorithms, the number of *floating point operations* (FLOPs), defined as a floating point addition, subtraction, multiplication, or division [27] between real numbers, are considered. Here, both the Hermitian and *if* conditional operators are disregarded. In a real implementation, some platforms may use hardware-based random number generators, where an electric circuit provides the random numbers; hence, the FLOP cost for random number generation was also disregarded in this analysis.

The FLOPs required for the main operations are summarized in Table 2 and the full complexity expressions are denoted by Υ. These values for the considered MIMO-OFDM detectors are presented in Table 3. To analyze the detectors' FLOP complexity for different numbers of antennas, Figure 10 depicts the linear and heuristic detector complexities assuming $N_{\text{dim}} = 2N_{\text{t}}$, $N_{\text{t}} = N_{\text{r}}$, and $N_{\text{ind}} = N_{\text{pop}} = 5N_{\text{dim}}$, and considering the number of iterations until convergence is obtained through simulations, as shown in Figures 4 and 6.

The ML detector computes all possible input matrices [6] resulting in the evaluation of (5) as $\mathcal{M}^{2N_{\text{t}}\times 1}$ times, where $\mathcal{M}$ represents the modulation order, making it the most computationally complex of the detectors considered. It can be observed that the DE algorithm requires more FLOPs than PSO since it evaluates two N_{pop} times the fitness function per iteration in (17) for individuals and crossover vectors. The complexity among the linear detectors is almost the same, differing by a scalar–matrix multiplication and matrix–matrix sum in (6) and (9).

TABLE 2 Number of FLOPs for vector and matrix operations: $\mathbf{w} \in \mathbb{R}^{q\times 1}, \mathbf{A} \in \mathbb{R}^{m\times q}, \mathbf{B} \in \mathbb{R}^{q\times p}, \mathbf{C} \in \mathbb{R}^{m\times p}, \mathbf{D} \in \mathbb{R}^{q\times q}$

Operation	# FLOPS
Matrix-matrix multiplication **AB**	$mp(2q-1)$
Matrix-vector multiplication **Aw**	$m(2q-1)$
Matrix multiply-add **AB** + **C**	$2mpq$
Square root $\sqrt{\cdot}$	8
Matrix inversion using LU factorization of **D** [28]	$2/3q^3 + q^2$
Norm-2, $\sqrt{\mathbf{w}^T\mathbf{w}}$	$2q - 1 + 8$

TABLE 3 Number of FLOPs per subcarrier for the MIMO-OFDM detectors, with $\mathcal{H} \in \mathbb{R}^{2N_{\text{r}}\times 2N_{\text{t}}}$, $\boldsymbol{\upsilon} \in \mathbb{R}^{2N_{\text{t}}\times 1}$, $N_{\text{dim}} = 2N_{\text{t}}$

Detector	Number of operations
$\Upsilon_{\text{ZF}}(N_{\text{t}}, N_{\text{r}})$	$\frac{16}{3}N_{\text{t}}^3 + 4N_{\text{t}}^3 + 32N_{\text{t}}^2N_{\text{r}} + 4N_{\text{t}}N_{\text{r}} - 2N_{\text{t}}$
$\Upsilon_{\text{MMSE}}(N_{\text{t}}, N_{\text{r}})$	$\frac{16}{3}N_{\text{t}}^3 + 8N_{\text{t}}^2 + 32N_{\text{t}}^2N_{\text{r}} + 4N_{\text{t}}N_{\text{r}}$
$\Upsilon_{\text{PSO}}(N_{\text{t}}, N_{\text{r}}, N_{\text{pop}}, \mathcal{I})$	$N_{\text{pop}}\mathcal{I}(8n_{\text{t}}N_{\text{r}} + 20N_{\text{t}} + 4N_{\text{r}} + 7)$
$\Upsilon_{\text{DE}}(N_{\text{t}}, N_{\text{r}}, N_{\text{ind}}, \mathcal{I})$	$N_{\text{ind}}\mathcal{I}(16N_{\text{t}}N_{\text{r}} + 12N_{\text{t}} + 8N_{\text{r}} + 14)$
$\Upsilon_{\text{ML}}(N_{\text{t}}, N_{\text{r}}, \mathcal{M})$	$\mathcal{M}^{2N_{\text{t}}}(8N_{\text{t}}N_{\text{r}} + 4N_{\text{r}} + 7)$

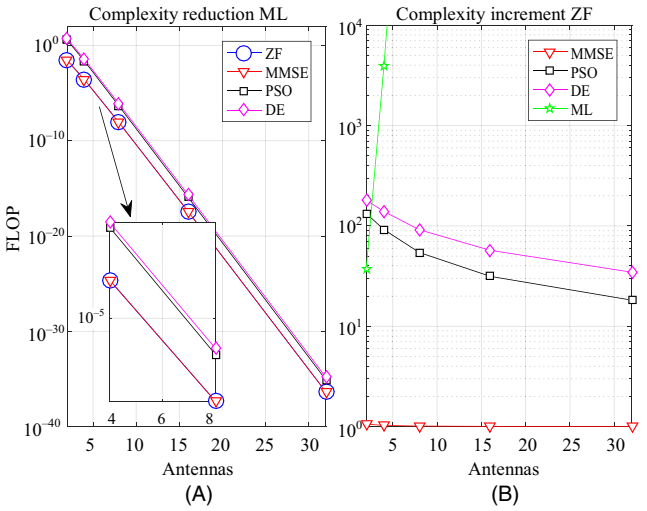

FIGURE 10 Relative complexity of MIMO-OFDM detectors considering different numbers of antennas for linear and heuristic detectors in a point-to-point scenario: $N_{\text{t}} = N_{\text{r}}$, $N_{\text{dim}} = 2N_{\text{t}}, N_{\text{ind}} = N_{\text{pop}} = 5N_{\text{dim}}, \mathcal{I} = 50, \mathcal{M} = 4$.

Relative complexity is depicted in Figure 10. On the left side, the complexity reduction relative to ML and linear/heuristic detectors, evaluated as $\Upsilon_{\text{det}}/\Upsilon_{\text{ml}}$, are shown. All the studied MIMO-OFDM detectors decrease complexity with respect to the ML detector. Note that PSO provides slightly more reduction than DE, and linear detectors provide more than the heuristics, at the cost of BER performance. On the right side, the complexity increases relative to the linear low-complexity ZF MIMO-OFDM detector $\Upsilon_{\text{det}}/\Upsilon_{\text{zf}}$ is determined. Note that the linear MMSE detector has a

complexity that is near to that of ZF resulting in values close to one, while the ML detector complexity increases rapidly as the number of antennas increases. The heuristic PSO detector increments complexity more slowly than the DE detector at almost the same BER performance, offering a good complexity tradeoff between computational complexity vs performance, mainly when the number of antennas increases (such as in massive MIMO systems).

6. | CONCLUSIONS

The analysis of an OFDM scheme was developed considering NLOS Rayleigh fading channel conditions. Extensive simulations were deployed and suitable input parameters for the evolutionary heuristics PSO and DE were chosen numerically for the MIMO-OFDM detection problem. The convergence of a PSO-based detector depends mainly on the E_b/N_0 level, requiring more iterations as the SNR increases.

Spatial correlation degrades the performance of the analyzed MIMO-OFDM detectors. For the uncorrelated scenario ($\rho = 0$), the PSO-aided detector outperforms linear detectors ZF and MMSE. However, for high correlation ($\rho = 0.9$), the PSO detector gain in terms of BER performance becomes marginal. The performance degradation as correlation increases is quantified by the sensitivity of the detectors for different levels of correlation.

Planar antenna arrays marginally outperform the linear array configurations for the ZF, MMSE, PSO, and DE MIMO-OFDM detectors considering high SNR operation region and low number of antennas. When the number of antennas increases, such outperformance may become noticeable. Although the correlation among antennas is slightly higher in the URA, this difference is not enough to deteriorate the performance of the system.

Comparing the complexity of the detector algorithms, the linear MMSE detector provides better performance than the linear ZF for almost the same computational complexity. Among the representative evolutionary heuristic MIMO-OFDM detectors, the PSO provides lower increments in complexity with respect to the DE detector, and almost the same (similar) BER performance for all the system and channel scenarios analyzed, both offering a suitable computational complexity vs performance tradeoff, even under medium spatial antenna correlation levels.

ACKNOWLEDGEMENTS

This work was supported in part by the National Council for Scientific and Technological Development (CNPq) of Brazil (Grants 130464/2015-5 and 304066/2015-0), in part by Araucaria Foundation, PR, (Grant 302/2012), and by Londrina State University - Paraná State Government, Brazil.

REFERENCES

1. L. L. Hanzo et al., *MIMO-OFDM for LTE, WiFi and WiMAX: Coherent versus non-coherent and cooperative turbo transceivers*, Wiley-IEEE Press, Torquay, UK, 2011.
2. G. Foschini and M. Gans, *On limits of wireless communications in a fading environment when using multiple antennas*, Wirel. Pers. Commun. **6** (1998), no. 3, 311–335.
3. E. Telatar, *Capacity of multi-antenna Gaussian channels*, Eur. Trans. Telecommun. **10** (1999), no. 6, 585–595.
4. M. A. Saeed, B. M. Ali, and M. H. Habaebi, *Performance evaluation of OFDM schemes over multipath fading channels, Asia-Pacific Conf. Commun. (IEEE Cat. No.03EX732)*, Penang, Malaysia, Sept. 21–24, 2003, pp. 415–419.
5. H. Steendam and M. Moeneclaey, *Analysis and optimization of the performance of OFDM on frequency-selective time-selective fading channels*, IEEE Trans. Commun. **47** (1999), no. 12, 1811–1819.
6. A. Goldsmith, *Wireless communications*, Cambridge University Press, New York, NY, USA, 2005.
7. J. R. Hampton, *Introduction to MIMO communications*, Cambridge University Press, New York, NY, USA, 2014.
8. A. Trimeche et al., *The particle swarm optimization (PSO) for symbol detection in MIMO-OFDM system*, Int. J. Inform. Secur. **4** (2013), no. 1, 38–45.
9. D. W. M. Guerra et al., Linear detection analysis in MIMO-OFDM with spatial correlation, *12th IEEE Int. Conf. Ind. Appicat. (INDUSCON)*, Curitiba, Brazil, 2016, pp. 1–8.
10. M. N. Seyman and N. Taspinar, *Symbol detection using the differential evolution algorithm in MIMO-OFDM Systems*, Turkish J. Elect. Eng Comp. Sci. **21** (2014), 373–380.
11. A. A. Khan, M. Naeem, and S. I. Shah, A particle swarm algorithm for symbols detection in wideband spatial multiplexing systems, *9th Annu. Conf. Genet. Evol. Comput. (GECCO '07)*, New York, NY, USA, 2007, pp. 63–69.
12. V. Zelst and J. Hammerschmidt, A single coefficient spatial correlation model for multiple-input multiple-output (Mimo) radio channels, *27th Gen. Assem. Int. Union Radio Sci. (URSI)*, Maastricht, Netherlands, Aug. 17–24, 2002, pp. 2–5.
13. G. Levin and S. Loyka, On capacity-maximizing angular densities of multipath in MIMO channels, *IEEE 72nd Veh. Tech. Conf.—Fall*, Ottawa, Canada, Sept. 2010, pp. 1–5.
14. J. Janhunen et al., *Fixed- and floating-point processor comparison for MIMO-OFDM detector*, IEEE J. Sel. Top. Signal Proc. **5** (2011) no. 8, 1588–1598.
15. A. P. R. N. D. Gore, *Introduction to space-time wireless communications*, Cambridge University Press, Cambridge, UK, 2003.
16. Y. S. Cho et al., *MIMO-OFDM wireless communications with MATLAB*, Wiley Publishing, Noida, India, 2010.
17. J. G. Proakis and M. Salehi, *Digital communications*, 5th ed., McGraw-Hill, New York, USA, 2008.
18. J. Kennedy and R. C. Eberhart, Particle swarm optimization, *IEEE Int. Conf. Neural Netw.*, Perth, Australia, Nov, 27-Dec. 1, 1995, pp. 1942–1948.
19. S. Cheng and Y. Shi, *Normalized population diversity in particle swarm optimization*, Springer Berlin Heidelberg, Berlin, Germany, 2011, pp. 38–45.
20. M. R. Bonyadi and Z. Michalewicz, *Particle swarm optimization for single objective continuous space problems: A review*, Evol. Comput. **25** (2017), no. 1, 1–54.

21. Y. Shi and R. C. Eberhart, Parameter selection in particle swarm optimization, *Evol. Prog. VII*, V. W. Porto, N. Saravanan, D. Waagen and A. E. Eiben, Eds., Springer Berlin Heidelberg, Berlin, Germany, 1998, pp. 591–600.
22. Y. Shi and R. Eberhart, A modified particle swarm optimizer, *IEEE Int. Conf. Evol. Comput. Proc. IEEE World Cong. Comput. Intell. (Cat. No. 98TH8360)*, Anchorage, AK, USA, May 4–9, 1998, pp. 69–73.
23. R. Storn and K. Price, *Differential evolution – A simple and efficient heuristic for global optimization over continuous spaces*, J. Glob. Optim. **11** (1997), no. 4, 341–359.
24. J. C. M. Filho, R. N. deSouza, and T. Abrão, *Ant colony input parameters optimization for multiuser detection in DS/CDMA systems*, Expert Sys. Appl. **39** (2012), no. 17, 12876–12884.
25. M. Clerc and J. Kennedy, *The particle swarm—Explosion, stability, and convergence in a multidimensional complex space*, IEEE Trans. Evol. Comput. **6** (2002), no. 1, 58–73.
26. I. C. Trelea, *The particle swarm optimization algorithm: Convergence analysis and parameter selection*, Inform. Proc. Lett. **85** (2003), no. 6, 317–325.
27. G. H. Golub and C. F. Van Loan, *Matrix computations*, 4th ed., Johns Hopkins University Press, Baltimore, USA, 2013.
28. S. Boyd and L. Vandenberghe, Numerical linear algebra background, available at http://www.seas.ucla.edu/~vandenbe/ee236b/lectures/num-lin-alg.pdf (Accessed Apr. 23, 2018).

AUTHOR BIOGRAPHIES

David William Marques Guerra received his BS degree in electrical engineering from the State University of Londrina, Brazil, in 2017, where he is currently working toward his MS degree in electrical engineering. His research interests lie in telecommunication systems, more precisely in wireless communications and signal processing, including multicarrier systems, MIMO systems, 5G, and the optimization aspects of communications systems and signals.

Rafael Masashi Fukuda received his BS degree in electrical engineering from the State University of Londrina, Brazil, in 2017. Currently, he is working on his MS degree in electrical engineering. His interests include OFDM and MIMO systems, 4G and 5G wireless systems, signal processing, and heuristics and convex optimization techniques for wireless communication systems.

Ricardo Tadashi Kobayashi received his BTech and MS degrees, both in electrical engineering, from the State University of Londrina, Brazil, in 2014 and 2016, respectively. Currently, he is working toward his PhD in electrical engineering at the State University of Londrina. His research interests lie in communications and signal processing, including MIMO detection techniques, optimization aspects of communications, convex optimization, and cognitive radio techniques.

Taufik Abrão received his BS degree, MSc degree, and PhD in electrical engineering from the Polytechnic School of the University of São Paulo, Brazil, in 1992, 1996, and 2001, respectively. Since March 1997, he has been with the Communications Group, Department of Electrical Engineering, Londrina State University, Brazil, where he is currently an associate professor in Telecommunications and the head of the Telecommunications and Signal Processing Lab. In 2012, he was an Academic Visitor with the Southampton Wireless Research Group, University of Southampton, UK. From 2007 to 2008, he was a postdoctoral researcher with the Department of Signal Theory and Communications, Polytechnic University of Catalonia, Spain. He has participated in several projects funded by government agencies and industrial companies. He is involved in editorial board activities of six journals in the telecommunications area and has served as a TPC member in several symposiums and conferences. He has also served as an editor for the *IEEE Communications Surveys and Tutorials* since 2013, *IEEE Access* since 2016, *IET Journal of Engineering* since 2014, and *ETT-Wiley* since 2016. He is a member of SBrT and a senior member of the IEEE. His current research interests include communications and signal processing, especially multiuser detection and estimation, MC-CDMA and MIMO systems, cooperative communication and relaying, resource allocation, as well as the heuristic and convex optimization aspects of 3G and 4G wireless systems. He has supervised 24 MSc degree and 4 PhD students, as well as 2 postdocs, co-authored nine book chapters on mobile radio communications and over 180 research papers published in specialized/international journals and conferences (http://www.uel.br/pessoal/taufik).